JOURNAL OF THERMOPHYSICS AND HEAT TRANSFER
Vol. 19, No. 4, October–December 2005

Validity of Hybrid Models for the Bidirectional Reflectance of Coated Rough Surfaces

Q. Z. Zhu,* H. J. Lee,* and Z. M. Zhang†
Georgia Institute of Technology, Atlanta, Georgia 30332-0405

Modeling of the bidirectional reflectance of thin-film coatings on rough surfaces has been an important and challenging problem. In the past, there have been studies that use thin-film optics to take account of the coating-induced interference effects and the geometric optics approximation to model the surface roughness. In an effort to delineate the validity regime of the hybrid method, the predicted bidirectional reflectance is compared with that obtained from the rigorous electromagnetic-wave solution for one-dimensional rough surfaces, considering the effect of coating thickness and roughness parameters. Two hybrid models are implemented using the Monte Carlo ray-tracing algorithm: the surface generation method and microfacet slope method. The former relies on statistically generated surfaces according to the root-mean-square roughness and the autocorrelation length, whereas the latter uses the microfacet whose orientation is stochastically determined, when a ray hits the surface, according to the slope distribution without creating deterministic rough surfaces a priori. The validity regimes of the hybrid models are established for silicon dioxide films on silicon substrates. The advantages and disadvantages of each hybrid model are discussed. Some useful guidelines are provided for the simulation of optical scattering from coated rough surfaces.

Nomenclature

d	=	local film thickness
E	=	bundle energy
f_r	=	bidirectional reflectance distribution function
H	=	y component of the magnetic field
h	=	average coating thickness
i	=	$\sqrt{-1}$
k_0	=	magnitude of wave vector in vacuum
L	=	normal derivative of H
l	=	length of a truncated surface
N	=	number of surface nodes
n	=	refractive index
p	=	probability density function
R_f	=	microfacet reflectance
r	=	Fresnel's reflection coefficient
W	=	weighting function
w	=	root-mean-square slope, $\sqrt{2\sigma/\tau}$
α	=	inclination angle
β	=	phase shift
ζ	=	microfacet slope
η	=	relative difference
θ	=	polar angle
λ	=	wavelength in vacuum
ξ	=	interface profile, $\xi(x)$
$\rho_{\mathrm{d-h}}$	=	reflectance
σ	=	root-mean-square roughness
τ	=	autocorrelation length

Subscripts

f	=	film
i	=	incidence
r	=	reflection
s	=	substrate
0	=	air

Presented as Paper 2004-2679 at the AIAA 37th Thermophysics Conference, Portland, OR, 28 June–1 July 2004; received 22 September 2004; revision received 30 November 2004; accepted for publication 4 December 2004.

*Graduate Research Assistant, George W. Woodruff School of Mechanical Engineering.

†Associate Professor, George W. Woodruff School of Mechanical Engineering; zzhang@mail.me.gatech.edu. Associate Fellow AIAA.

Introduction

THE study of radiation scattering from thin-film coated surfaces is very important in optical, materials, and thermal engineering.[1–7] Many optical components and semiconductor wafers are coated with thin films to meet the requirement of various applications. For example, silicon oxide, silicon nitride, and polysilicon are common materials used for thin-film layers on silicon wafers.[8] Models of radiative property for thin-film coated silicon wafers are essential to accurate temperature measuring in the semiconductor industry.[7–9] Although electromagnetic wave (EM-wave) theory of reflection from a multilayer system with ideally smooth interfaces has been well developed,[10] theoretical analyses and experimental measurements for scattering from a multilayer system with imperfect interfaces continue to be an active research area.[9] Some studies added a correction factor to Fresnel reflection coefficients to calculate the partially coherent reflectance and transmittance of a multilayer structure with rough interfaces.[1,11] Others applied the first-order vector perturbation theory[2,3] or the Kirchhoff approximation (see Refs. 12–15) to the simulation of scattering from multilayer systems. However, these methods are only applicable to either very smooth surfaces or slightly undulating surfaces.[2,12]

The geometric optics approximation (GOA) has been extensively used in analytical modeling and Monte Carlo simulation for scattering by rough surfaces.[6,7,16–21] A rough surface is regarded as an aggregate of randomly oriented microfacets. Each microfacet can be treated as a smooth surface, and the specular reflectance follows Fresnel's equations. Although it is generally believed that GOA is applicable when both the root-mean-square (rms) roughness and autocorrelation length are much greater than the wavelength, it has been verified that GOA is applicable even for surfaces whose roughness parameters are comparable to the wavelength.[18,19] Because GOA can lead to reasonable results for scattering by uncoated rough surfaces, it has been extended to simulate scattering by coated rough surfaces. When it is assumed that interference effects of the thin coating can be modeled by thin-film optics, Airy's formula could be used to calculate the microfacet reflectance (see Refs. 7 and 20). Because both GOA and thin-film optics are employed to model scattering by the coated rough surface, hereafter this approach is referred as the hybrid method.

The Monte Carlo ray-tracing method has been successfully applied to simulate scattering of radiation by opaque surfaces and semitransparent surfaces.[6,7,18,19] In the validity regime, where GOA agrees well with the EM-wave solution for uncoated surfaces, the Monte Carlo algorithm is computationally effective. The simulation using the hybrid models for coated surfaces requires very little extra computational effort. It was demonstrated that the prediction of the hybrid model agrees with the experimental result for absorbing films on a reflective substrate.[20] However, because the application of Airy's formula for each microfacet neglects the corner effect, there may be additional constraints for the hybrid models than for use of GOA alone in modeling rough surfaces without coating. It is imperative to establish the validity regime of the hybrid models to take full advantage of this method.

The ray-tracing approach can be undertaken by two methods, that is, the surface generation method (SGM)[18–20] and the microfacet slope method (MSM).[6,7,21] The main difference between these methods is the way to simulate rough surfaces. SGM numerically generates deterministic surfaces using two parameters, the rms roughness and autocorrelation length for a Gaussian surface before the ray tracing starts. On the other hand, MSM does not require a surface to be generated in advance; instead, it statistically determines the microfacet orientation, based on the slope distribution, each time when a ray hits the interface. Tang and Buckius[18] and Tang et al.[19,20] used SGM to predict the bidirectional reflectance of perfect conductors, dielectrics, and thin-film coated surfaces. Zhou and Zhang[6] and Lee et al.[7] used MSM to model radiative properties of thin-film coated opaque or semitransparent surfaces. SGM is more popular and can take full account of shadowing and multiple scattering, whereas MSM has some advantages in modeling scattering by semitransparent wafers with rough surfaces. Because the thickness of the wafer is on the order of hundreds of micrometers, approximately several thousand times smaller than the diameter, it is not feasible to generate a very large surface as required by SGM. Although the validity of SGM has been investigated in depth,[19] there has not been any study on the validity of MSM and the hybrid models based on either MSM or SGM.

Because the EM-wave solution is computationally demanding, this approach is practically applicable to one-dimensional rough surfaces only,[19,22,23] though solutions for two-dimensional rough surfaces have been obtained for some cases.[24] By the comparison of the EM-wave solution, validity regimes of the Kirchhoff approximation and GOA can be constructed (see Refs. 19 and 25). Although most available studies are for clean surfaces without a thin-film coating, Lu et al.[26] and Gu et al.[27] extended the EM-wave approach, based on the Green theorem and the extinction theorem to investigate backscattering by a multilayer system with rough interfaces. The present work applies the formulations developed in Refs. 26 and 27 to examine the validity of the hybrid models for scattering by one-dimensional thin-film coated rough surfaces. It is expected that the results will be qualitatively applicable for two-dimensional surfaces, which are mostly seen in the semiconductor industry. The validity regimes of the hybrid models will be established through comparison of simulation results from the rigorous EM-wave solution with those from the hybrid models. The consistency and discrepancy between the predicted results from SGM and MSM for Gaussian surfaces will also be examined.

Modeling and Simulation

The three-layer system with one-dimensional roughness and a thin-film coating is shown in Fig. 1. The surface profiles are invariable in the y direction. The film-substrate interface Σ_1 is described by $z = \xi_1(x)$, and its mean surface is located on the $z = 0$ plane. The air–film interface Σ_2 is described by $z = h + \xi_2(x)$, where h is the distance between the mean surfaces or the (average) coating thickness. The profile of the air–film interface is assumed to be identical to that of the film–substrate interface, that is, $\xi_1(x) = \xi_2(x)$. Although the actual interfaces may exhibit some deviation from the identical profile, the effect of interface correlation is not the focus of the present study. The ray is incident from air with a refractive index

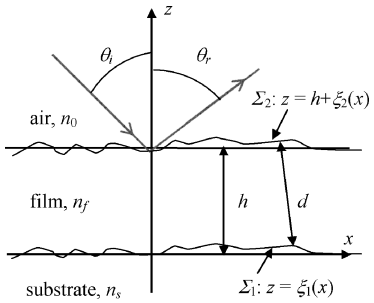

Fig. 1 Schematic of light scattering on three-layer system: profiles of the two interfaces assumed identical, that is, $\xi_1(x) = \xi_2(x)$, and refractive index n_f and n_s may be complex to include absorption.

$n_0 = 1$. The direction of incoming and outgoing beam is defined by the polar angles, θ_i and θ_r, respectively. The incidence direction, surface normal, and reflection direction are all parallel to the x–z plane. The substrate is assumed to be semi-infinite with a refractive index n_s. A thin-film coating with a refractive index n_f lies on top of the substrate, that is, $\xi_1(x) < z < h + \xi_2(x)$. For absorbing media, n_f and n_s will be complex.

In the Monte Carlo ray-tracing algorithm, a large number of ray bundles are illuminated on the rough surface, and each bundle is traced until it leaves the rough surface or is absorbed by the coated substrate. The rough surface consists of a large number of microfacets with different orientations. Some microfacets may not be illuminated if a bundle coming to the microfacet at oblique incidence is blocked by a neighboring microfacet. Similarly, the reflected bundle from the microfacet may be intercepted by its neighbor. These two events are referred as shadowing and restriking (masking), respectively. Restriking can occur successively, and thus, the intercepted bundle can be reflected back and forth between microfacets on the rough surface, causing multiple scattering. As a consequence, the incident radiation can be redirected to different directions by the microfacets through the first-order scattering and multiple scattering. For an uncoated surface, the reflectance of a microfacet is determined by Fresnel's equations according to the local incidence angle and refractive index of the medium (substrate). The bidirectional reflectance distribution function (BRDF) can be calculated by

$$f_r(\theta_i, \theta_r) = \frac{1}{E_i} \frac{\Delta E_r}{\cos\theta_r \Delta\theta_r} \tag{1}$$

where ΔE_r is the energy of the bundles reflected into the small angular range $\Delta\theta_r$ and E_i is the energy of all incoming bundles. The formulation for thin-film coated rough surfaces is essentially the same, except that, in the hybrid method, the microfacet reflectance is calculated from Airy's formula (see Refs. 20 and 28),

$$R_f = \left| \frac{r_{0f} + r_{fs} e^{-i2\beta}}{1 + r_{0f} r_{fs} e^{-i2\beta}} \right|^2 \tag{2}$$

where r_{0f} and r_{fs} are the Fresnel reflection coefficients at the air–film and film–substrate interfaces, respectively. The phase shift for wave traveling through the film is

$$\beta = 2\pi n_f d \cos\theta_f / \lambda \tag{3}$$

where θ_f is the refraction angle in the film. Because the microfacet is tilted by an inclination angle of α with respect to the mean surface, the local film thickness d is the projection of h to the microfacet normal; hence, $d = h\cos\alpha$.

Two different ray-tracing models are built based on the hybrid method to study light scattering by rough surfaces with coatings, that is, SGM and MSM. The height distribution function and autocorrelation function of the generated surfaces both are Gaussian, with an rms roughness σ and an autocorrelation length τ. Although the roughness statistics of real surfaces may deviate from the Gaussian (see Ref. 29), Gaussian statistics are used because the goal of the present study is to compare simulation results for the same random rough surface using different methods. Because MSM does not require a rough surface to be created, it will be discussed first.

In MSM, a microfacet is generated for each incoming ray bundle. The statistics of microfacet orientation is characterized by the slope distribution function. For a Gaussian surface, the slope distribution is also Gaussian with an rms slope $w = \sqrt{2}\,\sigma/\tau$, namely,[12]

$$p(\zeta) = \left(1/\sqrt{2\pi}\,w\right)\exp(-\zeta^2/2w^2) \tag{4}$$

where $\zeta = \mathrm{d}z/\mathrm{d}x$ is the microfacet slope. If the surface is divided into uniform intervals Δx in the x direction, the area projected to the horizontal plane will be the same for all microfacets. However, the energy illuminated on a given microfacet is proportional to the projected area of the microfacet toward the incidence direction. Therefore, the probability for a ray to strike a particular microfacet not only depends on the slope distribution but also on the incoming direction. A weighting function $W(\theta_i, \zeta)$ needs to be introduced to determine correctly the statistics of microfacet orientation. Because microfacets with $\zeta \le -1/\tan\theta_i$ do not face the incidence, the ray will never strike these microfacets, and thus, $W(\theta_i, \zeta) = 0$; otherwise, $W(\theta_i, \zeta) = \cos\theta_i + \zeta \sin\theta_i$ (Ref. 7). After normalization, the weighted probability density function of the microfacet orientation becomes

$$p_w(\zeta, \theta_i) = \frac{W(\theta_i, \zeta)p(\zeta)}{\int_{-\infty}^{\infty} W(\theta_i, \zeta)p(\zeta)\,\mathrm{d}\zeta} \tag{5}$$

Consequently, the occurrence probability of microfacet orientation is also dependent on the incoming direction. The rejection method is used to determine the orientation of the microfacet according to Eq. (5) using uniform random numbers; see Ref. 7 for a detailed discussion.

Ray bundles may not illuminate some microfacets on the rough surface because of shadowing. For microfacets with $\zeta \le -1/\tan\theta_i$ that do not face the incidence, shadowing will definitely occur and the weighting function in MSM takes care of this type of shadowing by setting $W(\theta_i, \zeta) = 0$. However, some microfacets facing the incidence may also be blocked (shadowed) by other surfaces. The weighting function does not take into account the influence of the shadowing by microfacets facing the incidence on the slope distribution of the illuminated surfaces. Therefore, MSM may not fully represent the shadowing effect for surfaces with a large rms slope at oblique incidence.

The algorithm for determining reflection and restriking is described as follows. Once the microfacet orientation is determined, the reflectance is calculated and a random number is created to decide whether the ray is absorbed or reflected. If the ray is reflected, it may hit another surface, which is called restriking. Because no physical surfaces are generated in MSM, the probability of restriking is needed. Smith[30] derived a shadowing function that depends on the propagating direction and the rms slope. This function was used in previous studies to model multiple scattering.[6,7,29] A new random number is used to decide if restriking occurs. If so, another microfacet is generated, and the same procedure to determine reflection and restriking is repeated until the bundle is either absorbed or leaves the rough surface. MSM is a fast ray-tracing technique that obeys the conservation of energy and the reciprocity principle.[7] However, because MSM only uses one roughness parameter w without generating a physical surface, the effect of restriking may not be correctly modeled, as will be discussed later.

The spectral method is used to generate rough surfaces in SGM. A sequence of uniform random numbers is generated and transformed into a sequence with normal statistics. The substrate surface profile $\xi_1(x)$ can be obtained after the new sequence is correlated with a Gaussian roughness spectrum according to the values of σ and τ (Refs. 22, 23, and 25). The generated deterministic surface is divided into many segments (microfacets). Each facet is represented by its center location as a node, and a large number of ray bundles are uniformly illuminated. There is no need to generate a physical interface for the air–film boundary in SGM because the reflectance is calculated from Eq. (2) considering the thin-film effect. The height and orientation of each microfacet can be calculated from the surface profile; therefore, shadowing and restriking are fully accounted for from the surface geometry using an iterative algorithm.[19] The generated surface is somewhat longer than the illuminated region to avoid the edge effect. The surface length cannot be arbitrarily large because the computational time increases approximately with the square of the number of nodes in SGM. Because of the limitation of the surface length, the discrepancy between individual surface realizations—rough surfaces generated from the same statistics—is unacceptable even though the number of ray bundles in the Monte Carlo simulation is sufficiently large. A common technique to overcome this difficulty is to obtain an ensemble average of the BRDF by repeating the ray tracing for a large number of realizations.[18–20]

The hybrid method may not represent the coated surface correctly because it does not physically generate the air–film interface. Figure 2 shows the section views of the rough interfaces for specific realizations of two surface statistics. The solid line indicates the profile of the substrate surface, whereas the broken lines indicate the profile of the film surfaces with different thicknesses. Thin-film optics assumes plane wave incident on smooth and flat surfaces whose lateral extension is infinite. When the surface is relatively shallow, as in Fig. 2a with an rms slope $w = \sqrt{2}\,\sigma/\tau \approx 0.14$, it is likely that the thin-film optics assumption is valid for each microfacet. For the case shown in Fig. 2b with $w = \sqrt{2}\,\sigma/\tau \approx 0.7$, however, the multiple reflected waves inside the film on a given microfacet may escape from the microfacet before they interfere with each other. As a result, the calculation of reflectance from Eq. (2) in both SGM and MSM may result in error for coated microfacets. This phenomenon is especially prominent near the corner and hereafter will be referred as the corner effect. It can be seen from Fig. 2b that the corner effect becomes more significant as h increases.

The EM-wave solution solves Maxwell's equations considering both the interfaces and is considered as a rigorous method. As shown in Fig. 1, because the plane of incidence is perpendicular to the y axis, the electromagnetic fields depend on x and z only. For p-polarized incidence, when the magnetic field vector is perpendicular to the plane of incidence, the reflected wave is also p polarized. When the extinction theorem using Green's function is applied, the magnetic fields inside air, film, and substrate are related to the incident field and the integrals of special functions along the interfaces Σ_1 and Σ_2 (Refs. 26 and 27). The magnetic field and its normal derivative (which is proportional to the tangential of the electric field) must be continuous at each interface as prescribed by the

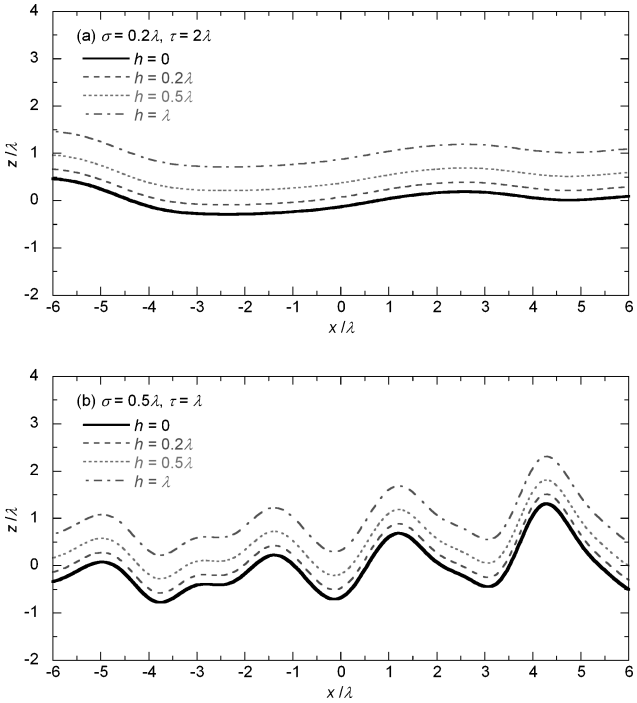

Fig. 2 Profiles of coated surfaces with increasing coating thickness: ——, interface between the film and substrate.

boundary conditions.[31] Transformations are then performed so that only the magnetic fields and their derivatives at the boundaries are involved in the solution.

The EM-wave approach uses the same method to generate the substrate surface $\xi_1(x)$ as in SGM. The air–film interface is generated by shifting the profile by h in the z direction because $\xi_1(x) = \xi_2(x)$ by assumption. Each surface profile is divided into N segments with equal interval Δx, and the projected surface length in the x direction is $l = N\Delta x$. The fields within each segment are assumed to be uniform. The unknowns are the magnetic fields $H^{(1)}(x_n)$ and $H^{(2)}(x_n)$ and their normal derivatives $L^{(1)}(x_n)$ and $L^{(2)}(x_n)$, at the two boundaries. Here, $x_n = (n - N/2)\Delta x$ with $n = 1, 2, \ldots, N$, and superscripts (1) and (2) stand for boundaries Σ_1 and Σ_2, respectively. Accordingly, the integral equations are converted into a coupled matrix equation with a dimension of $4N \times 4N$. This matrix is not sparse, and, consequently, the memory requirement and computational time for solving the matrix equation are formidable if the number of nodes on the rough surface is very large. After the matrix equation is solved, the reflection amplitude $r(\theta_r)$ can be calculated from the magnetic field and its normal derivative at the boundary Σ_2 (Refs. 22 and 23). Hence,

$$r(\theta_r) = \Delta x \sum_{n=1}^{N} \left\{ ik_0[\xi_1'(x_n)\sin\theta_r - \cos\theta_r]H^{(2)}(x_n) - L^{(2)}(x_n) \right\} \times \exp\{-ik_0[x_n \sin\theta_r + \xi_1(x_n)\cos\theta_r]\} \quad (6)$$

where $k_0 = 2\pi/\lambda$ is the magnitude of the wave vector in vacuum. For s polarization, the magnetic field and its normal derivative are replaced by the electric field and its normal derivative, respectively. The matrix elements for s polarization are different from those for p polarization because the boundary conditions have different forms. The BRDF for one-dimensional rough surfaces is[19,23]

$$f_r(\theta_i, \theta_r) = \frac{|r(\theta_r)|^2}{8\pi k_0 l \cos\theta_i \cos\theta_r} \quad (7)$$

Similar to SGM, because each surface realization cannot represent the scattering by the rough surface, ensemble averaging is also necessary to calculate the BRDF from the EM-wave solution.[24] Although the result for individual surface realization is not reliable, the ensemble-averaging method produces repeatable results for different sets of surface realizations within the standard deviation; hence, it is considered as a reliable and effective technique to model BRDF of rough surfaces.

Results and Discussion

Numerical Implementation and Validation Criterion

Computational codes are developed to simulate scattering by rough surfaces with or without thin-film coatings, based on the EM-wave approach. The simulation results for scattering by a perfectly conducting uncoated surface agree reasonably well with the experimental results in Ref. 32, and those for coated surfaces are identical to the results in Refs. 26 and 27. Furthermore, the reflectance of a thin silicon dioxide layer on top of a smooth silicon substrate is calculated and compared to the theoretical value obtained from Eq. (2). The average relative difference is less than 3% for p polarization and 1% for s polarization. The difference is attributed to the finite integral length and the finite number of surface nodes used in the EM-wave simulation.

In the numerical implementation of hybrid models, the angular resolution $\Delta\theta_r$ is set to 1 deg. SGM uses a finite surface ranging from 200λ to 250λ, depending on the rms surface roughness. Each surface consists of 2048 nodes. Only the 1000 nodes in the central region may intercept the incident radiation. Each node is checked by iteration to see whether it is shadowed by another surface node or not. For any surface node in the central region that is not shadowed, a ray bundle will be assigned and traced until it is leaves the surface (reflection) or is absorbed. Repeated tests have shown that 200 surface realizations are sufficient to ensure a relative standard deviation within 5% for BRDF values greater than 0.01. Although MSM does not require ensemble averaging, calculations are divided into groups. Each group includes 1000 ray bundles. Simulation results of 300–400 groups are averaged to achieve the standard deviation within 5%. In the EM-wave solution, usually the surface length is 40λ–60λ, and the surface is divided into 800–1000 nodes. The relative standard deviation is within 10% after averaging the BRDFs over 200 surface realizations.

A computer with a 3.2-GHz Pentium 4 processor and 2-GB memory is used in the simulation. For a perfectly conducting surface, it takes the computer a few seconds for MSM, about 6 min for SGM, and 30 min for the EM-wave solution. For a dielectric surface with a thin-film coating, it takes about 30 s for MSM, 5 min for SGM, and 9 h for the EM-wave solution. Because SGM applies a complicated iterative algorithm to deal with shadowing and restriking, it requires much more computational time than MSM does. Because a matrix equation needs to be solved, the EM-wave solution is rather computationally intensive. For a perfectly conducting surface, the tangential component of the electric field is zero at the air–surface interface. For a coated dielectric surface, the tangential components of both the electric and magnetic fields need to be solved by matching the boundary conditions at the air–film and film–substrate interfaces. Accordingly, the size of the matrix is $N \times N$ for a perfectly conducting surface, whereas it is $4N \times 4N$ for a thin-film coated surface. Therefore, the EM-wave solution for the coated surface is very time consuming. For simulations performed on the generated surfaces, the surface length and number of surface nodes are limited by the computational resource, and there is a tradeoff between the relative standard deviation and computational time. Conservation of energy is checked by calculating the directional–hemispherical reflectance and transmittance. The deviation of the reflectance from unity is less than 1% for perfectly conducting surfaces. For surfaces with dielectric coatings, the sum of the reflectance and transmittance deviates within 3% from unity.

Because thermal radiation is usually randomly polarized, the averaged BRDF values for p and s polarizations are used in the comparisons of simulation results. The EM-wave solutions are carried out for both polarizations separately, and then the calculated BRDFs are averaged. The ray-tracing methods apply the averaged reflectance for each microfacet and result in the BRDF for unpolarized incidence. Because the polarization state is maintained for one-dimensional rough surfaces, the ray-tracing methods are also capable of obtaining BRDF values for individual polarizations. Although the following discussion is for the unpolarized case only, the described procedure can be applied in developing validity regimes for individual polarizations. Three measures are used to quantify the difference between simulation results from the EM-wave solution and hybrid models. The overall difference is defined as

$$\eta_o = \frac{\int_{-\pi/2}^{\pi/2} |f_{r,\mathrm{EM}} - f_{r,\mathrm{HB}}| \cos\theta_r \, \mathrm{d}\theta_r}{\int_{-\pi/2}^{\pi/2} f_{r,\mathrm{EM}} \cos\theta_r \, \mathrm{d}\theta_r} \quad (8)$$

The hemispherical difference is defined as

$$\eta_h = \frac{\left| \int_{-\pi/2}^{\pi/2} (f_{r,\mathrm{EM}} - f_{r,\mathrm{HB}}) \cos\theta_r \, \mathrm{d}\theta_r \right|}{\int_{-\pi/2}^{\pi/2} f_{r,\mathrm{EM}} \cos\theta_r \, \mathrm{d}\theta_r} \quad (9)$$

The specular difference is defined as

$$\eta_s = \frac{\left| \int_{\theta_i - \theta_{\mathrm{hc}}}^{\theta_i + \theta_{\mathrm{hc}}} (f_{r,\mathrm{EM}} - f_{r,\mathrm{HB}}) \cos\theta_r \, \mathrm{d}\theta_r \right|}{\int_{\theta_i - \theta_{\mathrm{hc}}}^{\theta_i + \theta_{\mathrm{hc}}} f_{r,\mathrm{EM}} \cos\theta_r \, \mathrm{d}\theta_r} \quad (10)$$

where θ_{hc} is the half-cone angle, which is set to 5 deg. Subscripts o, h, and s in Eqs. (8–10) represent overall, hemispherical, and specular, respectively, and subscripts EM and HB stand for the EM-wave approach and hybrid models (either SGM or MSM), respectively. Each measure has its own merit depending on specific requirements. Here, η_h quantifies the difference of the directional–hemispherical reflectance, which is important when the radiative

power within the whole hemisphere is interested; η_s quantifies the difference of directional–conical reflectance, which is important when the radiative power within a small angular region around the specular direction is interested; and η_o emphasizes the accumulation of errors on each reflection angle within the region of $-\pi/2$–$\pi/2$. Hence, η_o can be considered as a more strict measure than η_h and η_s. In the present work, η_o is applied to evaluate the hybrid models, and the validation criterion is defined as $\eta_o < 20\%$.

Simulation on Perfectly Conducting Surfaces

Tang et al.[19] studied the validity of GOA for perfectly conducting uncoated surfaces using SGM and developed a validity regime on the basis of $\eta_o < 20\%$ in terms of two parameters: σ/τ and $\sigma \cos\theta_i/\lambda$. The ratio σ/τ, which is proportional to the rms slope w, cannot be very large; hence, $\sigma/\tau < 2$ is generally required for GOA to be valid. Although the simulation results using GOA are independent of wavelength because the reflectance of perfectly conducting surfaces is unity, σ must not be too small compared to the wavelength for GOA to be applicable. This requires that $\sigma \cos\theta_i/\lambda > 0.17$. Note that the boundaries of the validity regime in the $\sigma \cos\theta_i/\lambda - \sigma/\tau$ plot (Fig. 6 in Ref. 19) are not straight lines and the criteria $\sigma/\tau < 2$ and $\sigma \cos\theta_i/\lambda > 0.17$ vary slightly along the boundaries. Although both σ and τ are needed to characterize fully a Gaussian surface, the simulation result using GOA depends on the value of σ/τ only because proportional increase or decrease of both σ and τ will not affect the results. On the other hand, the EM-wave solution depends on both σ/λ and τ/λ.

As mentioned earlier, shadowing and restriking may not be well represented in MSM; this may further limit its applicable regime to even a smaller σ/τ range. The discussion in this section focuses on the validity of MSM and the difference between SGM and MSM. Surface roughness parameters are selected within the validity regime of GOA. Figure 3 shows a comparison of the simulation results for perfectly conducting surfaces. Note that the actual value of λ does not affect the result in this case, as long as σ/λ and τ/λ remain the same. Because the relative standard deviation of the EM-wave solution is 10%, the BRDF curves show noticeable statistical noise. The BRDF curves from SGM and MSM are smoother because their standard deviations are 5% only. The value σ/τ of 0.2 in Fig. 3a corresponds to an average microfacet inclination angle of 16 deg. For this surface, the chance of restriking (multiple scattering) is relatively small, and the first-order scattering dominates. The SGM and MSM simulation results agree well with each other and with the EM-wave solution. For the case shown in Fig. 3b with $\sigma/\tau = 1$, the average inclination angle is 55 deg, and restriking becomes significant. Although the BRDF predicted by MSM is lower in the angular region $|\theta_r| < 10$ deg, the overall difference η_o is within 20%. One can separate the first-, second-, and higher-order contributions from the total scattering in the SGM and MSM simulation results. Although the first-order contributions from SGM and MSM are very close, MSM predicts a larger contribution from multiple scattering than SGM does. Because at normal incidence shadowing does not occur in the first-order scattering, the comparison in Fig. 3b demonstrates that MSM has a limitation in modeling restriking when σ/τ is large. The reason may be due to limitation of the shadowing function that does not consider the correlation between height and slope.[28] In addition, the generation of the second microfacet, which intercepts the reflected bundle from the first microfacet, is independent of the orientation of the first microfacet. This may affect the prediction of the second-order or higher-order scatterings. Usually, the contribution of multiple scattering predicted by MSM is higher than that by SGM.

To investigate the limitation of MSM with regard to the shadowing effect, the simulation is repeated at $\theta_i = 30$ deg. As shown in Fig. 3c, for the surface with $\sigma/\tau = 0.2$, the MSM result agrees reasonably well with the SGM result and the EM-wave solution. For the surface with $\sigma/\tau = 1$, as shown in Fig. 3d, the MSM result significantly deviates from the EM-wave solution. The BRDF curves predicted by MSM look similar in Figs. 3c and 3d, even though θ_i changes from 0 to 30 deg. The overall difference for MSM η_o is 25%, and hence, MSM is not valid. On the other hand, SGM is valid with $\eta_o = 10\%$ even though it fails to predict the backscattering peak around $\theta_r = -\theta_i$. As mentioned earlier, the shadowing effect may not be fully represented in MSM. Furthermore, the error associated with restriking may increase with the incidence angle. From Fig. 3d, it can be inferred that the combination of restriking and shadowing can deteriorate the MSM simulation result.

The comparisons of simulation results show that MSM can result in reasonable agreement with the EM-wave solution when $\sigma/\tau < 1$ within the validity regime of SGM at normal incidence. Furthermore, the validity regime of MSM becomes more limited when the incoming radiation is from an oblique direction. The simulations are performed only at normal incidence and 30-deg incidence because a large incidence angle requires a very long surface and the EM-wave solution may be not accurate due to the edge effect.[19]

Simulation on Thin-Film Coated Surfaces

Silicon dioxide is a common dielectric film that can be grown by thermal oxidation or vapor deposition on silicon. In the present work, the coated surface consists of a thin layer of silicon dioxide on a silicon substrate with rough interfaces. Because silicon is opaque at room temperature when $\lambda < 1.1$ μm, the studied surface can be approximated by the three-layer system in Fig. 1. The refractive indexes of silicon dioxide and silicon are $n_f = 1.457$ and

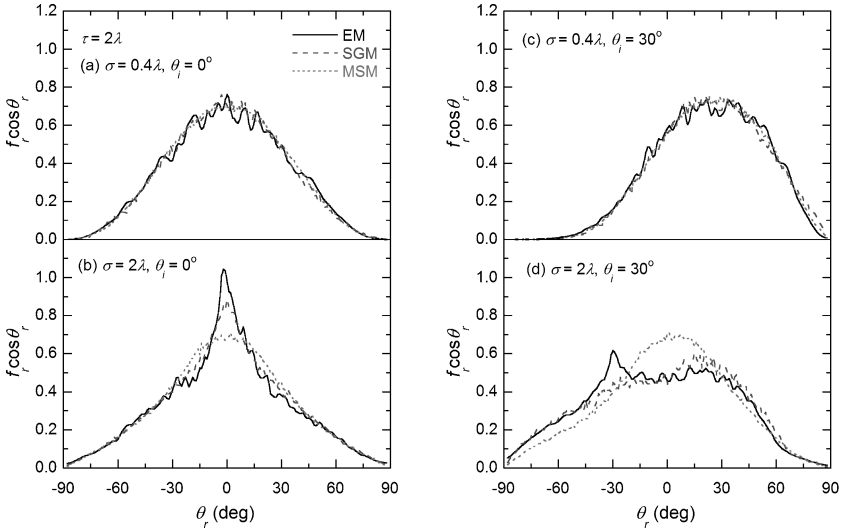

Fig. 3 Comparison of simulation results for scattering by perfectly conducting surfaces without coating for $\tau = 2\lambda$.

$n_s = 3.882 + 0.019i$ at $\lambda = 632$ nm (Ref. 33). Although only the wavelength of 632 nm is considered, the results should be applicable to wavelengths up to 1.1 μm because the optical constants of both materials do not change significantly. Table 1 lists the directional–hemispherical reflectance $\rho_{\text{d–h}}$ for coated surfaces, calculated from the EM-wave solution. As h increases, $\rho_{\text{d–h}}$ first goes down and then up, due to interference effects similar to the case of a smooth surface with coating. In addition, $\rho_{\text{d–h}}$ for coated surfaces are all smaller than that for the corresponding substrate. Figures 4–6 show the effects of coating thickness on the BRDFs calculated from the EM-wave solution and hybrid models. The simulation results for the substrate surface without coating are also shown for comparison. Detailed discussions are presented in the following paragraphs.

The roughness parameters of the substrate chosen in Fig. 4 are $\sigma = 0.2\lambda$ and $\tau = 2\lambda$. The simulation results at $\theta_i = 0$ deg are shown in Fig. 4a and those at $\theta_i = 30$ deg are shown in Fig. 4b. Because the value of $\sigma/\tau = 0.1$ is small, both hybrid models basically give the same results. Furthermore, the results from the EM-wave solution and hybrid models agree well when h is increased from 0 to λ. Quantitatively, the overall difference η_o is around 7% for both SGM and MSM at $h = \lambda$, and the standard deviation of the EM-wave solution is 6% for this case. It can also be seen from Fig. 4 that the peak of BRDF goes down and then up with increasing of h. This can be understood by the variation of the microfacet reflectance R_f with coating thickness due to interference effects. For example, when h increases from $0, 0.1\lambda, 0.2\lambda, 0.5\lambda$, to λ, the R_f for normal incidence changes from 0.349, 0.205, 0.110, 0.093, to 0.335, consecutively. Because BRDF is proportional to R_f, the BRDF value at the specular direction, $\theta_i = \theta_r = 0$ deg, first goes down and then up. It can be seen from the first column of Table 1 that $\rho_{\text{d–h}}$ follows the same trend and is close to R_f for the same coating thickness. The same conclusion can be drawn for $\theta_i = 30$ deg, except slight angular shifts in certain BRDF peaks from the specular direction of $\theta_r = 30$ deg.

The rms roughness of the substrate used in Fig. 5 is $\sigma = 0.5\lambda$, whereas τ is the same as that in Fig. 4. Figure 5 shows no obvious deviation between the SGM and MSM simulation results at $\sigma/\tau = 0.25$. This is consistent with the conclusions for perfectly conducting surfaces. The peak value of BRDF goes down and then up when h increase from 0.1λ to 0.5λ. The third and fourth columns of Table 1 show a similar trend for $\rho_{\text{d–h}}$, except for the case with $\theta_i = 30$ deg and $h = \lambda$. Besides the change of the peak values, the shape of the BRDF curves varies significantly as h increases. The BRDF curves for $h = 0.1\lambda$ have a bell-like shape. However, the shapes for $h = 0.5\lambda$ and $h = \lambda$ are very different. Two satellite peaks can be observed around $|\theta_r| = 50$ deg in the BRDF curve for $h = 0.5\lambda$ at $\theta_i = 0$ deg. In the BRDF curve for $h = 0.5\lambda$ and $\theta_i = 30$ deg, there exist a peak at $\theta_r = 52$ deg and a shoulder around $\theta_r = -22$ deg. The BRDF values at the satellite peaks and off-specular peaks can be higher than that at the specular direction. For $\sigma/\tau = 0.25$, the major contribution to the scattering is from the first order. Therefore, the occurrence of the satellite peaks and off-specular peaks can be explained by the variation of the microfacet reflectance R_f. Take $\theta_i = 0$ deg and $h = 0.5\lambda$ as an example. The inclination angle for the first-order reflection is determined by $\alpha = \theta_r/2$ because $\theta_i = 0$ deg. Therefore, the reflectance is $R_f = 0.09$ for the specular reflection $\theta_r = 0$ deg with a local film thickness $d = 0.5h$. Because both d and θ_f depend on α, it can be shown that $R_f = 0.23$ at $\theta_r = 50$ deg. Although the maximum of R_f occurs at $\theta_r > 50$ deg, the peak of $f_r \cos\theta_r$ is around $\theta_r = 50$ deg because both probability of microfacet orientation and $\cos\theta_r$ decreases rapidly as θ_r increases.

Figure 5 shows that the agreement between the simulation results from the EM-wave solution and hybrid models is good when h is up to 0.5λ. At $h = 0.5\lambda$, the overall difference is around 10% for both SGM and MSM, and the standard deviation of the EM-wave solution is around 7%. When h is increased to λ, satellite peaks observed in the BRDF curves from the hybrid models are not obvious in the curves from the EM-wave solution; these peaks are replaced by shoulders with smaller magnitudes. The agreement between the EM-wave solution and hybrid models is good when $|\theta_r| < 50$ deg at $\theta_i = 0$ deg, and the specular difference is less than 7%. Although some deviations can be observed in the region $60 < |\theta_r| < 80$ deg,

Table 1 Variation of directional–hemispherical reflectance $\rho_{\text{d–h}}$ with coating thickness and roughness parameters at $\lambda = 632$ nm

	$\sigma = 0.2\lambda, \tau = 2\lambda$		$\sigma = 0.5\lambda, \tau = 2\lambda$		$\sigma = 0.5\lambda, \tau = \lambda$	
h	$\theta_i = 0$ deg	$\theta_i = 30$ deg	$\theta_i = 0$ deg	$\theta_i = 30$ deg	$\theta_i = 0$ deg	$\theta_i = 30$ deg
0	0.349	0.348	0.344	0.337	0.274	0.293
0.1λ	0.212	0.228	0.221	0.226	0.180	0.201
0.2λ	0.104	0.094	0.098	0.088	0.069	0.090
0.5λ	0.104	0.158	0.150	0.180	0.125	0.157
λ	0.306	0.206	0.216	0.144	0.131	0.126

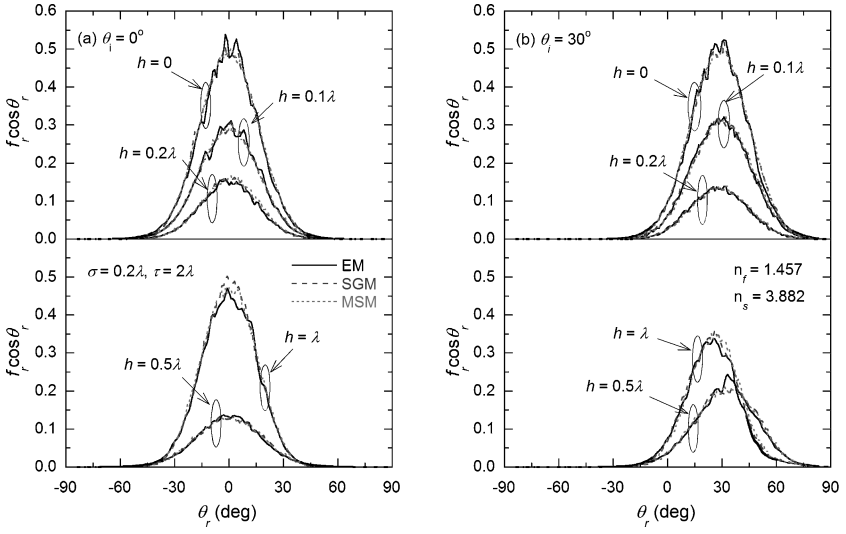

Fig. 4 Effects of coating thickness on the BRDF for $\sigma = 0.2\lambda$ and $\tau = 2\lambda$, where $\lambda = 632$ nm.

Table 2 Overall, hemispherical, and specular differences η_o: η_h: η_s (%) for both hybrid models when $h = 0.1\lambda$ and $\lambda = 632$ nm

	$\tau = \lambda$		$\tau = 2\lambda$		$\tau = 4\lambda$	
Condition	$\theta_i = 0$ deg	$\theta_i = 30$ deg	$\theta_i = 0$ deg	$\theta_i = 30$ deg	$\theta_i = 0$ deg	$\theta_i = 30$ deg
$\sigma = 0.1\lambda$						
SGM	34:1:33[a]	50:1:41[a]	25:2:13[a]	35:2:17[a]	13:1:1	18:8:6
MSM	33:2:34[a]	50:1:42[a]	26:2:14[a]	35:2:17[a]	11:1:1	17:8:6
$\sigma = 0.2\lambda$						
SGM	6:1:5	14:3:12	5:2:1	6:2:8	7:2:4	5:2:1
MSM	7:1:7	15:2:12	5:2:2	6:2:8	8:2:5	5:2:1
$\sigma = 0.5\lambda$						
SGM	13:8:13	13:6:20	7:1:4	10:1:1	11:3:11	10:2:12
MSM	10:1:15	8:1:12	6:2:1	7:2:2	11:2:13	11:2:10
$\sigma = \lambda$						
SGM	9:1:14	12:1:10	7:1:11	11:1:12	12:5:13	10:1:11
MSM	13:8:26	23:9:2[a]	10:5:15	10:5:4	12:4:7	10:3:9

[a]Here η_o is greater than 20%.

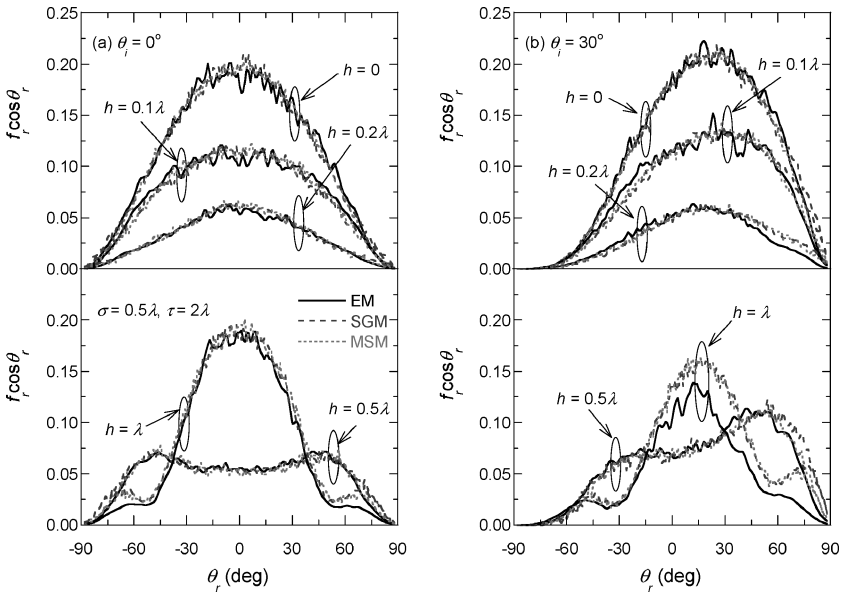

Fig. 5 Effects of coating thickness on the BRDF for $\sigma = 0.5\lambda$ and $\tau = 2\lambda$.

the hybrid models are still valid because $\eta_o \approx 16\%$. However, at $\theta_i = 30$ deg and for $h = \lambda$, both SGM and MSM overpredict the BRDF for $\theta_r > -10$ deg, and the hybrid models are invalid because $\eta_o \approx 36\%$.

The BRDF simulation results for $\sigma = 0.5\lambda$ and $\tau = \lambda$ are compared in Fig. 6. Note that the corresponding ρ_{d-h} values are given in the fifth and sixth columns in Table 1. The peak of BRDF also decreases when h is increased from 0 to 0.2λ. The agreement in the simulation results is reasonable for $h \leq 0.2\lambda$. Because of the relatively large value of σ/τ in this case, the BRDF curves display backscattering peaks in most cases, and significant deviations occur between the simulation results for $h = 0.5\lambda$. Quantitatively, η_o for SGM is 36% at $\theta_i = 0$ deg and 27% at $\theta_i = 30$ deg, whereas that for MSM is 27% and 13%, respectively. The deviation in the simulated BRDFs for surfaces with $h = \lambda$ is even larger and, hence, not shown in Fig. 6. It can be inferred that the hybrid model is not applicable for $h \geq 0.5\lambda$ for $\sigma/\tau \geq 0.5$.

A large number of variables, such as the rms roughness, autocorrelation length, refractive indexes of substrates and coatings, and coating thickness, are involved in the simulation. Constructing a complete validity regime for coated rough surfaces is not feasible. In the present work, the validity of hybrid models is examined for silicon dioxide coating on silicon at the wavelength of 632 nm. The rms roughness σ is varied from 0.1λ to λ and the autocorrelation length τ from λ to 4λ. Some of the combinations are intentionally selected near the boundary of the validity regime of GOA[19] to show how the validity regime of the hybrid method will be different from that of GOA. The differences between the EM-wave solution and hybrid-model predictions for both the normal incidence and 30-deg incidence are presented in Tables 2, 3, and 4 for $h = 0.1\lambda$, 0.5λ, and λ, respectively. The validity regime for uncoated surfaces is very similar to that for surfaces coated with $h = 0.1\lambda$ film because the corner effect is insignificant. All three differences (η_o, η_h, and η_s) are listed for each case, and cases with $\eta_o > 20\%$ are noted to emphasize that either SGM or MSM is invalid. For $h = 0.1\lambda$ as shown in Table 2, the differences for MSM and SGM are very similar. However, MSM is not valid when $\sigma = \lambda$ and $\tau = \lambda$ at $\theta_i = 30$ deg because of the shadowing and restriking effects. As discussed earlier, for GOA to be valid, $\sigma \geq 0.2\lambda$. Therefore, $\sigma = 0.1\lambda$ is too small for GOA to be valid, and the hybrid model is also not applicable to these cases, except for $\tau = 4\lambda$, which will be discussed later.

As shown in Table 3 for $h = 0.5\lambda$, in addition to the cases when $\sigma = 0.1\lambda$, the hybrid method is not valid for several cases when $\tau = \lambda$. The poor agreement between simulation results is caused by the deviation around the satellite peaks at normal incidence and around the off-specular peaks at oblique incidence, as shown in Fig. 6. As expected, when h increases to 0.5λ, the validity regime of the hybrid models is significantly reduced because the corner effect is more significant. However, the influence is not as large for $\tau = 2\lambda$ or 4λ when the average inclination angle is small. Meanwhile, the

Table 3 Overall, hemispherical, and specular differences η_o: η_h: η_s (%) for both hybrid models when $h = 0.5\lambda$

	$\tau = \lambda$		$\tau = 2\lambda$		$\tau = 4\lambda$	
Condition	$\theta_i = 0$ deg	$\theta_i = 30$ deg	$\theta_i = 0$ deg	$\theta_i = 30$ deg	$\theta_i = 0$ deg	$\theta_i = 30$ deg
$\sigma = 0.1\lambda$						
SGM	36:1:33[a]	51:3:42[a]	24:1:13[a]	33:2:14[a]	13:1:1	18:2:1
MSM	37:2:34[a]	51:3:42[a]	24:2:13[a]	32:2:14[a]	11:1:1	17:2:1
$\sigma = 0.2\lambda$						
SGM	18:10:15	26:14:12[a]	7:2:6	8:2:11	5:1:2	8:2:3
MSM	18:9:16	24:11:14[a]	7:2:5	7:2:8	6:2:2	7:2:3
$\sigma = 0.5\lambda$						
SGM	36:30:23[a]	27:26:15[a]	10:3:10	12:3:6	8:3:5	11:3:5
MSM	27:8:45[a]	13:12:3	6:1:9	8:1:5	8:3:8	10:3:7
$\sigma = \lambda$						
SGM	18:18:16	28:25:23[a]	18:14:16	12:7:9	10:4:4	10:1:5
MSM	15:14:36	14:1:8	11:4:41	8:5:3	12:6:1	11:5:4

[a]Where η_o is greater than 20%.

Table 4 Overall, hemispherical, and specular differences η_o: η_h: η_s (%) for both hybrid models when $h = \lambda$

	$\tau = \lambda$		$\tau = 2\lambda$		$\tau = 4\lambda$	
Condition	$\theta_i = 0$ deg	$\theta_i = 30$ deg	$\theta_i = 0$ deg	$\theta_i = 30$ deg	$\theta_i = 0$ deg	$\theta_i = 30$ deg
$\sigma = 0.1\lambda$						
SGM	37:4:25[a]	56:8:27[a]	23:2:5[a]	46:17:6[a]	12:2:3	27:2:3[a]
MSM	37:4:27[a]	56:9:28[a]	25:2:7[a]	46:17:6[a]	12:1:2	28:3:3[a]
$\sigma = 0.2\lambda$						
SGM	15:15:5	14:7:3	6:3:10	7:4:6	10:2:12	9:2:8
MSM	14:14:1	13:6:4	6:3:4	7:4:5	8:2:10	8:2:7
$\sigma = 0.5\lambda$						
SGM	48:46:4[a]	51:41:25[a]	17:17:6	37:34:52[a]	11:5:13	9:3:11
MSM	37:36:3[a]	46:31:20[a]	15:15:1	35:33:49[a]	9:5:13	9:4:8
$\sigma = \lambda$						
SGM	23:8:21[a]	65:60:91[a]	36:34:2[a]	58:58:72[a]	13:13:15	11:5:8
MSM	23:14:25[a]	48:36:50[a]	26:25:2[a]	47:47:60[a]	11:10:13	10:3:6

[a]Where η_o is greater than 20%.

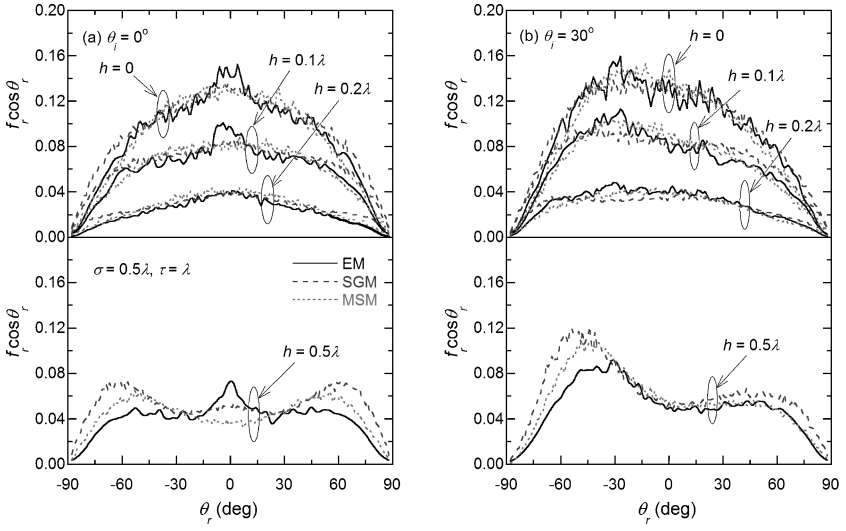

Fig. 6 Effects of coating thickness on the BRDF for $\sigma = 0.5\lambda$ and $\tau = \lambda$.

average size of the microfacet is still large because to some extent τ is related to the mean lateral dimension of the microfacets. In some cases with $\tau = \lambda$, MSM can result in better agreement with the EM-wave solution than SGM. For example, in the case of $\sigma = 0.5\lambda$, $\tau = \lambda$, and $\theta_i = 30$ deg, η_o is 27% for SGM and 13% for MSM. In general, SGM is better than MSM if there is no film on the surface. The probability of restriking may be overpredicted by MSM, and ray bundles have more chance to be absorbed by the surface, resulting in smaller BRDF values at large reflection angles. In the case of thin-film coated surfaces, the corner effect can degrade the accuracy of SGM simulations, but both the corner effect and restriking can affect the MSM predictions. When the coating thickness and σ/τ are large, SGM may overpredict the BRDF due to corner effect. On the contrary, the overpredicted restriking may counteract the influence of corner effect in the MSM simulations. Therefore, the relative difference between the hybrid-model results and the EM-wave solution becomes smaller for MSM.

Table 4 presents the differences in the simulation results for surfaces with $h = \lambda$. The validity regime for SGM is basically identical to that for MSM. Note that the validity regime of the hybrid models

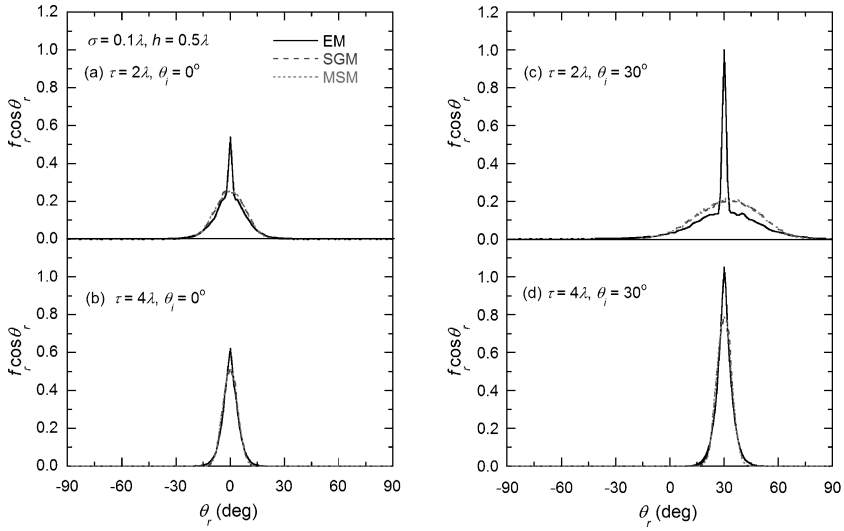

Fig. 7 Effects of autocorrelation length on the BRDF for $\sigma = 0.1\lambda$ and $h = 0.5\lambda$.

has been significantly reduced for thick films. Most of the cases in the region $0.5\lambda \le \sigma \le \lambda$ and $\lambda \le \tau \le 2\lambda$ are invalid. This is attributed to the relatively large value of σ/τ. The hybrid models are valid in the region of $\sigma = 0.2\lambda$ and $\tau \ge \lambda$ and in the region of $0.2\lambda \le \sigma \le \lambda$ and $\tau \ge 4\lambda$.

According to the validity regime of GOA, $\sigma = 0.1\lambda$ is an invalid case. However, as shown in Tables 2 and 3, although the hybrid models fail for surfaces with $\sigma = 0.1\lambda$ and $\tau = \lambda$ (or 2λ), they are valid for surfaces with $\sigma = 0.1\lambda$ and $\tau = 4\lambda$. Figure 7 shows a comparison of the BRDFs for surfaces with $\sigma = 0.1\lambda$ and $h = 0.5\lambda$ when τ increases from 2λ to 4λ. In Fig. 7a, where $\tau = 2\lambda$, the BRDF value from the hybrid models is much lower than that from the EM-wave solution at $\theta_r = 0$ deg. Although η_h is only 2%, η_o is greater than 20%; therefore, the hybrid models are not valid for this case. However, in Fig. 7b, where $\tau = 4\lambda$, the BRDF value from the hybrid models is close to that from the EM-wave solution, and η_o of the hybrid models is approximately 12%, which is within the validation criterion. The same transition can be observed at $\theta_i = 30$ deg, as shown in Figs. 7c and 7d. The reason for higher specular peaks at $\theta_r = 30$ deg, compared to those at $\theta_r = 0$ deg, is because rough surfaces appear smoother to oblique incidence. Although the transition of validity does not occur at $\sigma = 0.1\lambda$ and $\theta_i = 30$ deg in Table 4, η_o is significantly reduced. Therefore, increasing τ will reduce the differences between the hybrid method and the EM-wave solution.

Conclusions

This work investigates the validity of the hybrid models for the simulation of scattering by thin-film coated rough surfaces and examines the difference between two hybrid models. Although MSM is faster, SGM has advantages over MSM because the generated surface profile allows accurate determination of shadowing and re-striking. MSM is applicable to surfaces with $\sigma/\tau < 1$ at normal incidence, and the applicable regime becomes smaller at oblique incidence. The validity of the hybrid models is evaluated by comparison of the simulation results to the rigorous EM-wave solution, for silicon dioxide films on silicon substrates with one-dimensional roughness. Both the coating thickness and the value of σ/τ can significantly affect the validity of the hybrid method because of the corner effect. If the substrate has a large σ/τ, the hybrid method is only valid when the coating thickness is much less than the wavelength. Based on the criterion $\eta_o < 20\%$, the validity regime of the hybrid models is $0.2\lambda \le \sigma \le \lambda$ and $\tau \ge 2\lambda$ when $h = 0.1\lambda$ and 0.5λ. When $h = \lambda$, however, the validity regime is significantly reduced. Increasing τ can reduce η_o, and for $\tau = 4\lambda$, the hybrid models are valid even when $\sigma = 0.1\lambda$ for most cases, except when $h = \lambda$ and $\theta_i = 30$ deg. This study theoretically justifies that the hybrid method can be applied over certain ranges of roughness parameters and coating thickness. Although the comparisons are performed for one-dimensional rough surfaces only, the findings can provide some general guidelines for the application of the hybrid method to practical two-dimensional rough surfaces. The developed validity regimes will benefit future research related to the radiative properties of thin-film coated rough surfaces.

Acknowledgments

This work was supported by the National Science Foundation (Grants CTS-0236831 and CTS-0331153 subcontracted from the Florida Institute of Technology) and the Georgia Institute of Technology Focused Research Program. The authors thank Kakuen Tang, Pei-feng Hsu, and J. Robert Mahan for valuable comments.

References

[1]Filinski, I., "The Effects of Sample Imperfections on Optical Spectra," *Physica Status Solidi. B*, Vol. 49, No. 2, 1972, pp. 577–588.

[2]Elson, J. M., "Infrared Light Scattering from Surfaces Covered with Multiple Dielectric Overlayers," *Applied Optics*, Vol. 16, No. 11, 1977, pp. 2872–2881.

[3]Bruno, W. M., Roth, J. A., Burke, P. E., Hewitt, W. B., Holmbeck, R. E., and Neal, D. G., "Prediction of the Bidirectional Reflectance-Distribution Function from Atomic-Force and Scanning-Tunneling Microscope Measurements of Interfacial Roughness," *Applied Optics*, Vol. 34, No. 7, 1995, pp. 1229–1238.

[4]Giovannini, H., and Amra, C., "Scattering-Reduction Effect with Overcoated Rough Surfaces: Theory and Experiment," *Applied Optics*, Vol. 36, No. 22, 1997, pp. 5574–5579.

[5]Shen, Y. J., Zhang, Z. M., Tsai, B. K., and DeWitt, D. P., "Bidirectional Reflectance Distribution Function of Rough Silicon Wafers," *International Journal of Thermophysics*, Vol. 22, No. 4, 2001, pp. 1311–1326.

[6]Zhou, Y. H., and Zhang, Z. M., "Radiative Properties of Semitransparent Silicon Wafers with Rough Surfaces," *Journal of Heat Transfer*, Vol. 125, No. 3, 2003, pp. 462–470.

[7]Lee, H. J., Lee, B. J., and Zhang, Z. M., "Modeling the Radiative Properties of Semitransparent Wafers with Rough Surfaces and Thin-Film Coatings," *Journal of Quantitative Spectroscopy and Radiative Transfer*, Vol. 93, Nos. 1–3, 2005, pp. 185–194.

[8]Timans, P. J., Sharangpani, R., and Thakur, R. P. S., "Rapid Thermal Processing," *Handbook of Semiconductor Manufacturing Technology*, edited by Y. Nishi and R. Doering, Marcel Dekker, New York, 2000, pp. 201–286.

[9]Zhang, Z. M., Fu, C. J., and Zhu, Q. Z., "Optical and Thermal Radiative Properties of Semiconductors Related to Micro/Nanotechnology," *Advances in Heat Transfer*, Vol. 37, 2003, pp. 179–296.

[10]Yeh, P., *Optical Waves in Layered Media*, Wiley, New York, 1988, Chaps. 4, 5.

[11]Mitsas, C. L., and Siapkas, D. I., "Generalized Matrix Method for Analysis of Coherent and Incoherent Reflectance and Transmittance of Multilayer Structures with Rough Surfaces, Interfaces, and Finite Substrate," *Applied Optics*, Vol. 34, No. 10, 1995, pp. 1678–1683.

[12]Beckmann, P., and Spizzichino, A., *The Scattering of Electromagnetic Waves from Rough Surfaces*, Artech House, Norwood, MA, 1987, Chap. 3.

[13]Icart, I., and Arques, D., "Simulation of the Optical Behavior of Rough Identical Multilayer," *Proceedings of SPIE*, Vol. 4100, 2000, pp. 84–95.

[14]Lettieri, T. R., Marx, E., Song, J.-F., and Vorburge, T. V., "Light Scattering from Glossy Coatings on Paper," *Applied Optics,* Vol. 30, No. 30, 1991, pp. 4439–4447.

[15]McKnight, M. E., Vorburge, T. V., Mara, E., Nadal, M. E., Barnes, P. Y., and Galler, M., "Measurement and Prediction of Light Scattering by Clear Coatings," *Applied Optics,* Vol. 40, No. 13, 2001, pp. 2159–2168.

[16]Torrance, K., and Sparrow, E., "Theory for Off-specular Reflection from Roughed Surfaces," *Journal of the Optical Society of America,* Vol. 57, No. 9, 1967, pp. 1105–1114.

[17]Smith, T. F., and Hering, R. G., *Bidirectional Reflectance of a Randomly Rough Surface*, AIAA Progress in Astronautics and Aeronautics, Vol. 29, MIT Press, Cambridge, MA, 1972, pp. 69–85.

[18]Tang, K., and Buckius, R. O., "The Geometric Optics Approximation for Reflection from Two-Dimensional Random Rough Surfaces," *International Journal of Heat and Mass Transfer*, Vol. 41, No. 13, 1998, pp. 2037–2047.

[19]Tang, K., Dimenna, R. A., and Buckius, R. O., "Regions of Validity of the Geometric Optics Approximation for Angular Scattering from Very Rough Surfaces," *International Journal of Heat and Mass Transfer*, Vol. 40, No. 1, 1997, pp. 49–59.

[20]Tang, K., Kawka, P. A., and Buckius, R. O., "Geometric Optics Applied to Rough Surfaces Coated with an Absorbing Thin Film," *Journal of Thermophysics and Heat Transfer*, Vol. 13, No. 2, 1999, pp. 169–176.

[21]Prokhorov, A. V., and Hanssen, L. M., "Algorithmic Model of Microfacet BRDF for Monte Carlo Calculation of Optical Radiation Transfer," *Proceedings of SPIE*, Vol. 5192, 2003, pp. 141–157.

[22]Maradudin, A., Michel, T., McGurn, A. R., and Méndez, E. R., "Enhanced Back-Scattering of Light from a Random Grating," *Annals of Physics*, Vol. 203, No. 2, 1990, pp. 255–307.

[23]Sánchez-Gil, J. A., and Nieto-Vesperinas, M., "Light Scattering from Random Rough Dielectric Surfaces,"*Journal of the Optical Society of America. A*, Vol. 8, No. 8, 1991, pp. 1270–1283.

[24]Saillard, M., and Sentenac, A., "Rigorous Solutions for Electromagnetic Scattering from Rough Surfaces," *Waves in Random Media*, Vol. 11, No. 3, 2001, pp. R103–R137.

[25]Thorsos, E., "The Validity of the Kirchhoff Approximation for Rough Surface Scattering Using a Gaussian Roughness Spectrum," *Journal of the Acoustical Society of America*, Vol. 83, No. 1, 1988, pp. 78–92.

[26]Lu, J. Q., Maradudin, A. A., and Michel, T., "Enhanced Backscattering from a Rough Dielectric Film on a Reflection Substrate," *Journal of the Optical Society of America. B*, Vol. 8, No. 2, 1991, pp. 311–318.

[27]Gu, Z.-H., Lu, J. Q., and Maradudin, A. A., "Enhanced Backscattering from a Rough Dielectric Film on a Glass Substrate," *Journal of the Optical Society of America. A*, Vol. 10, No. 8, 1993, pp. 1753–1764.

[28]Modest, M. F., *Radiative Heat Transfer*, McGraw–Hill, New York, 1993, Chap. 2.

[29]Zhu, Q. Z., and Zhang, Z. M., "Anisotropic Slope Distribution and Bidirectional Reflectance of a Rough Silicon Surface," *Journal of Heat Transfer*, Vol. 126, No. 6, 2004, pp. 985–993.

[30]Smith, B., "Geometrical Shadowing of a Random Rough Surface," *IEEE Transactions on Antennas and Propagation*, Vol. 15, No. 5, 1967, pp. 668–671.

[31]Born, M., and Wolf, E., *Principles of Optics*, 7th ed., Cambridge Univ. Press, Cambridge, England, U.K., 1999, Chap. 1.

[32]Kim, M.-J., Dainty, J. C., Friberg, A. T., and Sant, A. J., "Experimental Study of Enhanced Backscattering from One- and Two-Dimensional Random Rough Surfaces," *Journal of the Optical Society of America. A*, Vol. 7, No. 4, 1990, pp. 569–577.

[33]Palik, E. D., *Handbook of Optical Constants of Solids*, Academic Press, Orlando, FL, 1985, pp. 546–569, 749–763.